Measurement of the ^{2}H(^{7}Be, ^{6}Li)^{3}He reaction rate and its contribution to the primordial lithium abundance*

Er-Tao Li(李二涛)[1,2;1)] Zhi-Hong Li(李志宏)[1;2)] Sheng-Quan Yan(颜胜权)[1] Jun Su(苏俊)[1] Bing Guo(郭冰)[1] Yun-Ju Li(李云居)[1] You-Bao Wang(王友宝)[1] Gang Lian(连钢)[1] Sheng Zeng(曾晟)[1] Si-Zhe Chen(陈思泽)[3] Shao-Bo Ma(马少波)[3] Xiang-Qing Li(李湘庆)[4] Cao He(何超)[4] Hui-Bin Sun(孙慧斌)[2] Wei-Ping Liu(柳卫平)[1]

[1] China Institute of Atomic Energy, Beijing 102413, China
[2] College of Physics and Energy, Shenzhen University, Shenzhen 518060, China
[3] Institute of Modern Physics, Chinese Academy of Sciences, Lanzhou 730000, China
[4] School of Physics and State Key Laboratory of Nuclear Physics and Technology, Peking University, Beijing 100871, China

Abstract: In the standard Big Bang nucleosynthesis (SBBN) model, the lithium puzzle has attracted intense interest over the past few decades, but still has not been solved. Conventionally, the approach is to include more reactions flowing into or out of lithium, and study the potential effects of those reactions which were not previously considered. ^{7}Be(d, ^{3}He)^{6}Li is a reaction that not only produces ^{6}Li but also destroys ^{7}Be, which decays to ^{7}Li, thereby affecting ^{7}Li indirectly. Therefore, this reaction could alleviate the lithium discrepancy if its reaction rate is sufficiently high. However, there is not much information available about the ^{7}Be(d, ^{3}He)^{6}Li reaction rate. In this work, the angular distributions of the ^{7}Be(d, ^{3}He)^{6}Li reaction are measured at the center of mass energies $E_{\rm cm}$ = 4.0 MeV and 6.7 MeV with secondary ^{7}Be beams for the first time. The excitation function of the ^{7}Be(d, ^{3}He)^{6}Li reaction is first calculated with the computer code TALYS and then normalized to the experimental data, then its reaction rate is deduced. A SBBN network calculation is performed to investigate its influence on the ^{6}Li and ^{7}Li abundances. The results show that the ^{7}Be(d, ^{3}He)^{6}Li reaction has a minimal effect on ^{6}Li and ^{7}Li because of its small reaction rate. Therefore, the ^{7}Be(d, ^{3}He)^{6}Li reaction is ruled out by this experiment as a means of alleviating the lithium discrepancy.

Keywords: reaction rates, primordial lithium abundance, big bang nucleosynthesis, lithium puzzles

PACS: 25.70.Hi, 25.60.Je, 26.35.+c **DOI:** 10.1088/1674-1137/42/4/044001

1 Introduction

In 1982, the Spites found that lithium abundance in metal-poor stars appears to be a plateau, independent of metallicity and effective temperature, according to astronomical observations, and the mean value is about log$\varepsilon_{\rm Li}$ = 2.05 ± 0.15 dex [1] in the scale of log$\varepsilon_{\rm H}$ = 12 dex. Later, the lithium plateau was confirmed by other works and new results are mainly between 2.0 and 2.3, which agree with the Spites value [2–9]. The lithium plateau observed in metal-poor stars must originate in Big Bang nucleosynthesis (BBN). With the development of observational technology, the abundances of ^{6}Li and ^{7}Li can be separated [9–13] and the ratio is about 5%, which means that the abundances of ^{6}Li and ^{7}Li are about log$\varepsilon_{^6{\rm Li}}$ ≈ 0.8 dex and log$\varepsilon_{^7{\rm Li}}$ ≈ 2.1 dex respectively. According to the standard BBN (SBBN) model, the abundances of elements only depend on the baryon-photon ratio η. Using the precise value of η = (6.203 ± 0.137) × 10^{-10} [14–16] determined by the Wilkinson Microwave Anisotropy Probe (WMAP), the abundances of ^{2}H, ^{3}He and ^{4}He are successfully predicted within 1% error [17, 18]. However, the abundance of ^{7}Li is predicted to be log$\varepsilon_{^7{\rm Li}}$ ≈ 2.6 dex, about a factor of three higher than the observational value. Even worse, the abundance of ^{6}Li is predicted to be log$\varepsilon_{^6{\rm Li}}$ ≈ -2.5 dex, which is approximately three orders of magnitudes lower than the observationally determined value. These problems are called the lithium puzzle. They have attracted a lot of attention in astrophysics because this can help us to explore the conditions of the early universe and test various cosmological models [19].

The lithium puzzle is one of the most important issues in the field, and brings new challenges to astronomical

Received 14 November 2017, Revised 13 January 2018, Published online 6 March 2018

∗ Supported by National Natural Science Foundation of China (11375269, 11505117, 11490560, 11475264, 11321064), Natural Science Foundation of Guangdong Province (2015A030310012), 973 program of China (2013CB834406) and National key Research and Development Province (2016YFA0400502)

1) E-mail: let@szu.edu.cn

2) E-mail: zhli@ciae.ac.cn

observation and model calculation. To solve the problem, we need to improve both astronomical observations and model calculations [20, 21]. Hou et al. [22] modified the velocity distributions of nuclei during the BBN era and found excellent agreement between predicted and observed primordial abundance of ^{7}Li, but did not provide any information about ^{6}Li. From BBN calculations, we can try to include as many lithium-involving reactions as possible to study the potential effects of those reactions which were not considered previously. Even though attempts to resolve the discrepancies by using this conventional nuclear physics method have been unsuccessful over the past few decades, altering the reactions flowing into and out of lithium is still being proposed [23–25].

^{7}Be is a neighbor nucleus of both ^{6}Li and ^{7}Li. Its abundance is about one order of magnitude higher than that of ^{7}Li and four orders of magnitude higher than that of ^{6}Li in the BBN era. The study of reactions involving ^{7}Be may offer a profound understanding of the lithium puzzle. The ^{7}Be(d, ^{3}He)^{6}Li reaction not only produces ^{6}Li but also destroys ^{7}Be, that decays to ^{7}Li, and thereby affects ^{7}Li indirectly. To date, however, there has been no experimental data for the ^{7}Be(d, ^{3}He)^{6}Li reaction. Its effect on the ^{7}Li and ^{6}Li abundances was evaluated by using the ^{7}Be(d,p)2^{4}He reaction rate. If the unknown ^{7}Be(d, ^{3}He)^{6}Li reaction rate is assumed to be the same as the ^{7}Be(d,p)2^{4}He reaction rate, SBBN calculations show that it results in a decrease or increase in abundance of about 1% for ^{7}Li or ^{6}Li, respectively. If the ^{7}Be(d, ^{3}He)^{6}Li reaction rate is artificially multiplied by a factor of 100, the SBBN calculations show that ^{7}Li decreases 45% and ^{6}Li increases 47%. However, it remains to be investigated whether its reaction rate is sufficiently high to alleviate the lithium discrepancy.

In the present work, the angular distributions of the ^{7}Be(d, ^{3}He)^{6}Li reaction at center of mass energies $E_{\rm cm}$ = 4.0 MeV and 6.7 MeV are measured separately for the first time by using the secondary beam facility of the HI-13 tandem accelerator at the China Institute of Atomic Energy (CIAE), Beijing. The integrated cross sections of the ^{7}Be(d, ^{3}He)^{6}Li reaction are obtained. With the nuclear reaction code TALYS [26], the excitation function is obtained. The reaction rate at energies of astrophysical interest is also deduced. To investigate the effect of ^{7}Be(d, ^{3}He)^{6}Li on the ^{6}Li and ^{7}Li abundances, SBBN network calculations are performed and the fluxes of the reactions connecting to ^{6}Li and ^{7}Li isotopes are compared.

2 Measurement of angular distributions

The experiment was carried out at the radioactive secondary beam facility [27] of the HI-13 tandem accelerator at the CIAE, Beijing. The experimental setup is similar to previous [28–30] experiments, as shown in Fig. 1. The 37 MeV and 46 MeV ^{7}Li primary beams from the tandem accelerator impinged on a H_2 gas cell at 1.5 atm pressure, separately. The front and rear windows of the gas cell are Havar foils with thickness 1.9 mg/cm^2. The ^{7}Be ions were produced via the ^{1}H(^{7}Li, ^{7}Be)n reaction. After magnetic separation with a dipole and focusing with a quadruple doublet, the ^{7}Be secondary beams were further purified by a Wien filter, and then delivered and collimated by two apertures of diameter 5 mm and 3 mm to limit the beam spot size. In order to monitor the beam purity and distinguish ^{7}Be from contaminants for later gating, a 19.3 μm-thick silicon ΔE_1 detector and a 23.0 μm-thick silicon ΔE_2 detector were placed upstream of the secondary target. The typical primary ^{7}Li beam intensity is about 70 pnA and the secondary ^{7}Be beam intensity is approximately 5000 pps with a purity of 99%. As an example, a contour plot of the ΔE_1 vs ΔE_2 detectors is shown in Fig. 2. One can see that there are small amounts of ^{4}He and ^{7}Li contaminants which can be discriminated by the correlation data of the ΔE_1 and ΔE_2 detectors.

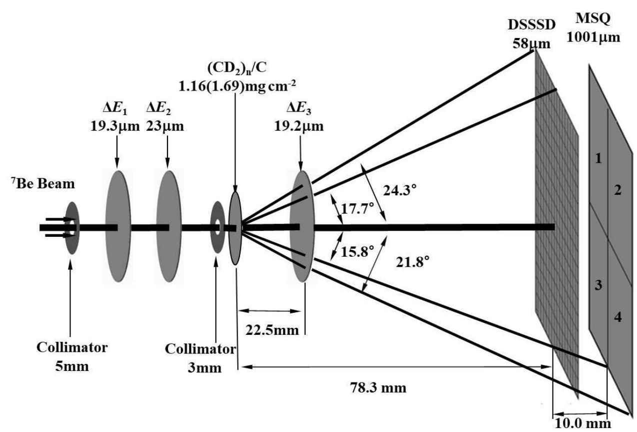

Fig. 1. Schematic layout of the experimental setup.

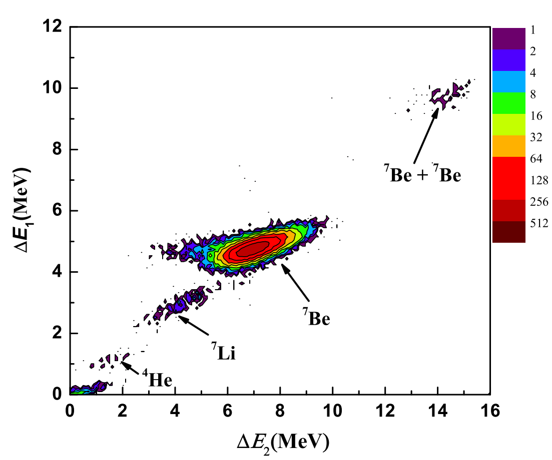

Fig. 2. (color online) Contour plot of ΔE_1 vs ΔE_2 at $E_{\rm lab}$(^{7}Li) = 37 MeV.

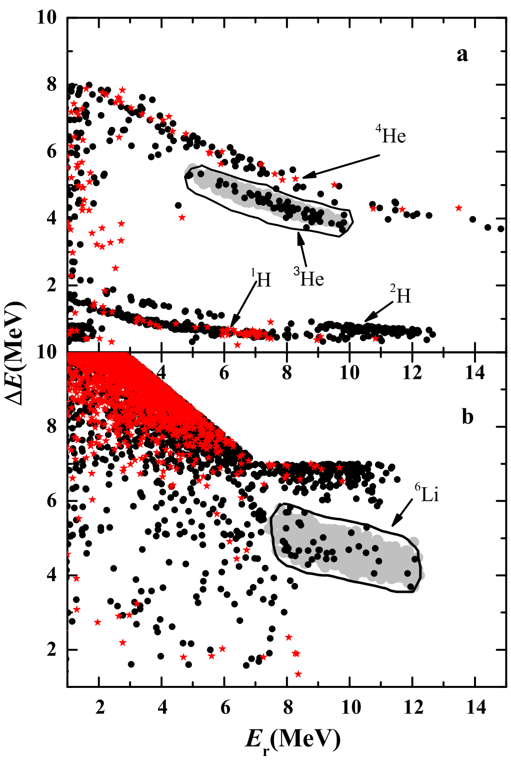

Fig. 3. (color online) ΔE vs $E_{\rm r}$ scatter plots of $(CD_2)_n$ target (black solid spots) and pure carbon target (red solid stars) at $E_{\rm cm} = 4.0$ MeV. For ^{3}He ions (top panel), ΔE vs $E_{\rm r}$ was measured by the DSSSD and MSQ detectors. For ^{6}Li ions (bottom panel), ΔE vs $E_{\rm r}$ was measured by the ΔE_3 and DSSSD detectors and the MSQ detector was used as veto. The grey areas are the kinematics regions of the Monte Carlo simulations. The two-dimensional gates were used to obtain the ^{3}He and ^{6}Li ions based on the Monte Carlo simulations. For the bottom plot, there are too many events above $\Delta E > 7$ MeV, so for the sake of saving CPU time in dealing with the experimental data, some of those events are cut.

A 1.16 mg/cm^2 $(CD_2)_n$ foil and a 1.69 mg/cm^2 pure carbon foil served as a secondary target to measure the ^{7}Be(d, ^{3}He)^{6}Li reaction and to evaluate the background, respectively. The energies of ^{7}Be ions at the middle of the $(CD_2)_n$ target were 17.7 MeV and 30.2 MeV, corresponding to the energies of 4.0 MeV and 6.7 MeV in the center of mass frame. After the secondary target, a 19.2 μm-thick silicon ΔE_3 detector was placed at 22.5 mm downstream to perform particle identification and beam normalization. A 58 μm-thick double-sided silicon strip detector (DSSSD) and a 1001 μm-thick quadrant silicon detector (MSQ) forming a ΔE–$E_{\rm r}$ counter telescope was placed 78.3 mm downstream of the secondary target to detect ^{6}Li ions at $E_{\rm cm} = 6.7$ MeV and ^{3}He ions at both $E_{\rm cm} = 4.0$ MeV and 6.7 MeV. ^{6}Li ions at $E_{\rm cm} = 4.0$ MeV cannot penetrate the DSSSD detector, so the ΔE_3 and DSSSD detectors composing a ΔE vs $E_{\rm r}$ counter telescope was used to measure them. Here, ΔE is the energy measured by the transmission detector and $E_{\rm r}$ is the residual energy.

Both DSSSD and MSQ detectors are 50 mm × 50 mm in size. The DSSSD is divided into 16 strips of 3 mm width on the front face, with 0.1 mm gaps, and 16 orthogonal strips with the same geometry on the back face, making up 256 pixels of 3 mm × 3 mm each, to provide quasi-pixel two dimensional position information. Therefore, the DSSSD has a position resolution of 3 mm × 3 mm, defined by the width of the micro-strips orthogonally oriented on both sides. The MSQ is a 2 × 2 array of independent active area, separated by a 0.1 mm cross gap. Under the geometry shown in Fig. 1, such a detector configuration covers the laboratory angular range from 0° to 21.8°.

As examples, Fig. 3 and Fig. 4 show ΔE vs $E_{\rm r}$ scatter plots at $E_{\rm cm} = 4.0$ MeV and 6.7 MeV, respectively. The two-dimensional gates were drawn based on Monte Carlo simulation. The simulation took the beam spot size, geometrical factor, resolution of the detectors, angular and energy straggling effects in the target and detectors into account. After background subtraction and beam normalization, the angular distributions of the ^{7}Be(d, ^{3}He)^{6}Li reaction were obtained as shown in Fig. 5. The forward angle data come from the measurement of ^{6}Li ions and the backward angle data come from the measurement of ^{3}He ions. The errors result from the uncertainty of target thickness (5%) and the statistics (10%–67%, depending on angle).

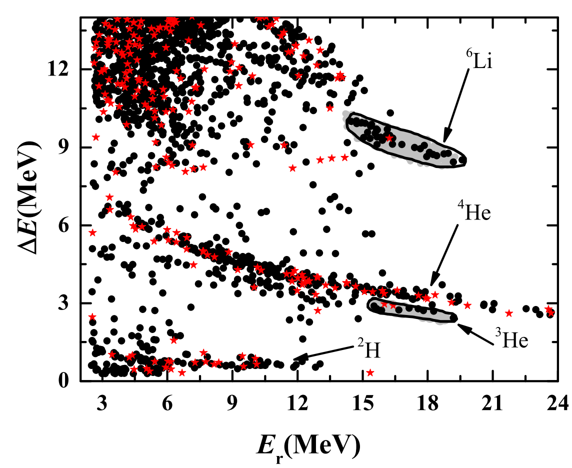

Fig. 4. (color online) ΔE vs $E_{\rm r}$ scatter plots of $(CD_2)_n$ target (black solid spots) and pure carbon target (red solid stars) at $E_{\rm cm} = 6.7$ MeV, ΔE vs $E_{\rm r}$ was measured by the DSSSD and MSQ detectors. The grey areas are the kinematics regions of the Monte Carlo simulations. The two-dimensional gates were used to obtain the ^{3}He and ^{6}Li ions based on the Monte Carlo simulations.

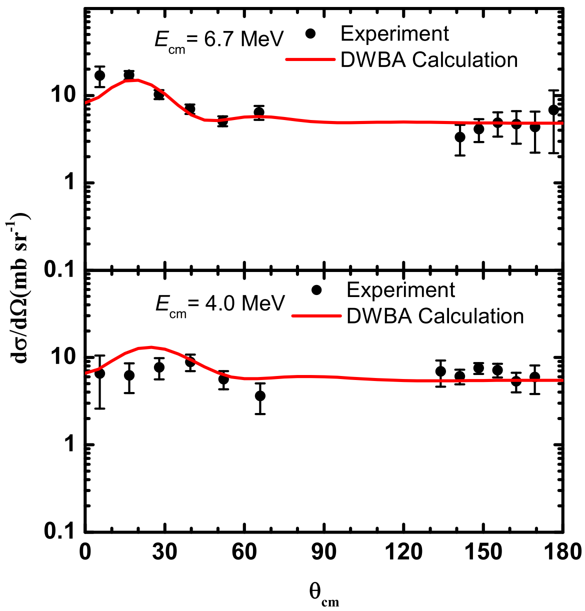

Fig. 5. (color online) Angular distributions of the ^{7}Be(d, ^{3}He)^{6}Li reaction at $E_{\rm cm}$ = 4.0 MeV and $E_{\rm cm}$ = 6.7 MeV. The black points with errors are the experimental cross sections, and the red dashed curves represent the DWBA calculations.

3 The astrophysical ^{7}Be(d, ^{3}He)^{6}Li reaction rate

To deduce the total cross sections, the differential cross sections are simply connected and integrated to be 73.3 ± 22.1 mb and 73.1 ± 15.8 mb at $E_{\rm cm}$ = 4.0 MeV and $E_{\rm cm}$ = 6.7 MeV, respectively. The ^{7}Be(d, ^{3}He)^{6}Li angular distributions are also reproduced by the distorted wave Born approximation (DWBA) method with the TWOFNR code [31] as shown in Fig. 5. The optical model potential (OMP) parameters with Woods-Saxon form are listed in Table 1. The proton spectroscopic factors of the $p3/2$ and $p1/2$ components in ^{7}Be used in the DWBA calcualtions are 0.43 and 0.29 [32], respectively. Because of the low incident energy, the compound nuclear reaction mechanism is also considered in the DWBA calculations. Comparing with the linear fitting method, the integrated cross sections obtained by the DWBA method are increased by 10% at $E_{\rm cm}$ = 4.0 MeV and decreased by less than 1% at $E_{\rm cm}$ = 6.7 MeV.

The energies of the experiment are much higher than the required Gamow window data. To get the important Gamow window data, the excitation function was firstly calculated with the computer code TALYS [26] and then normalized to the experimental data points. The normalizing factor is 1.35. The pre-equilibrium contribution successfully used in other works [33] is considered in the TALYS calculation. The experimental data and the normalized excitation function are shown in Fig. 6.

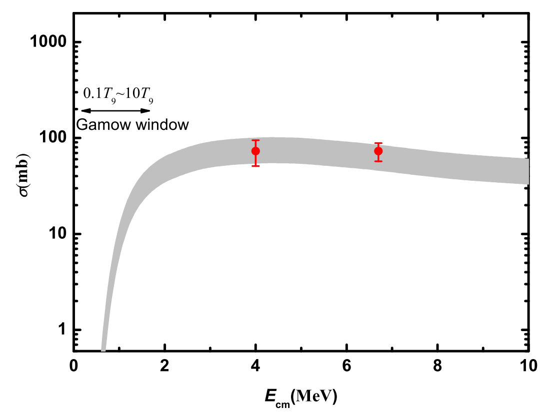

Fig. 6. (color online) The excitation function of the ^{7}Be(d, ^{3}He)^{6}Li reaction. The red points with errors represent the experimental data, and the black curve is the normalized excitation function.

The astrophysical reaction rate is calculated with

$$N_{\rm A}\langle\sigma\nu\rangle = N_{\rm A}\left(\frac{8}{\pi\mu}\right)^{1/2}\frac{1}{(k_{\rm B}T)^{3/2}} \times\int_0^\infty \sigma(E)E\exp\left[-\frac{E}{k_{\rm B}T}\right]{\rm d}E, \quad (1)$$

where ν is the relative velocity of ^{7}Be and d, $\sigma(E)$ is the excitation function, μ is the reduced mass of the ^{7}Be + d system, and $N_{\rm A}$ and $k_{\rm B}$ are the Avogadro and Boltzmann constants respectively. For convenience, the rate is fitted with the expression used in the astrophysical reaction rate library REACLIB [34],

$$N_{\rm A}\langle\sigma\nu\rangle = \exp[12.8885-4.37376\ T_9^{-1}+28.7918\ T_9^{-\frac{1}{3}} -29.9038\ T_9^{\frac{1}{3}}+0.647569\ T_9 -0.013777\ T_9^{\frac{5}{3}}+21.5953\ln(T_9)], \quad (2)$$

where T_9 is the temperature in units of GK. The overall fitting errors are less than 1% at temperatures from 0.05 to 50 GK.

Table 1. OMP parameters used in the DWBA calculations, from Ref. [35]. $E_{\rm cm}$ denotes the energy in MeV for the relevant channels, V and W are the depths in MeV, and r and a are the radius and diffuseness in fm.

channel	$E_{\rm cm}$	V	r_v	a_v	W	r_w	a_w	$W_{\rm s}$	$r_{\rm s}$	$a_{\rm s}$	$V_{\rm so}$	$r_{\rm so}$	$a_{\rm so}$	$r_{\rm C}$
d + ^{7}Be	4.0/6.7	95.7	1.05	0.86				59.6	1.43	0.55	3.5	0.75	0.50	1.30
^{3}He + ^{6}Li	3.9	150.9	1.20	0.72	39.8	1.40	0.88				2.5	1.20	0.72	1.30
^{3}He + ^{6}Li	6.6	150.2	1.20	0.72	38.4	1.40	0.88				2.5	1.20	0.72	1.30

4 BBN calculations

In the SBBN calculation, the dynamics of primordial nucleosynthesis is controlled by a cosmological parameter: the baryon-to-photon ratio η, which is precisely measured to be 6.203 $\times$ 10^{-10} [14] by WMAP. The neutron lifetime of $t_{1/2}$ = 613.9 s [36] is adopted in our calculation. The reaction network used in the SBBN calculation involves 34 reactions with nuclei of $A \leqslant 7$. The calculation begins at a temperature of $T_9 = 50$, at which the abundances of the nuclei are fixed by statistical equilibrium.

The reaction network calculation was performed with a modified code from Wagoner's computational routines [37]. For the reaction $N_i(^{A_i}Z_i)+N_j(^{A_j}Z_j) \longleftrightarrow N_k(^{A_k}Z_k)+N_l(^{A_l}Z_l)$, the reaction net flux of nucleus i can be calculated by

$$\begin{aligned}\int_{t_1}^{t_2}\frac{\mathrm{d}Y_i}{\mathrm{d}t}\mathrm{d}t &= \int_{t_1}^{t_2}\Big(-\frac{\mathrm{d}Y_{i\to k}}{\mathrm{d}t}+\frac{\mathrm{d}Y_{k\to i}}{\mathrm{d}t}\Big)\mathrm{d}t\\ &= \int_{t_1}^{t_2}N_i\Big(-\frac{Y_i^{N_i}Y_j^{N_j}}{N_i!N_j!}[ij]_k+\frac{Y_l^{N_l}Y_k^{N_k}}{N_l!N_k!}[lk]_i\Big)\mathrm{d}t.\end{aligned} \tag{3}$$

where Y_i is the mole fraction of nucleus i, N_i is the number of such nuclei involved in this reaction, $[ij]_k = (\rho_\mathrm{b}N_\mathrm{A})^{N_i+N_j-1}\ \langle ij\rangle$, ρ_b is the baryon density and $\langle ij\rangle$ represents the reaction rate between i and j. In case of decay, N_j and N_l will be zero. The reaction forward flow is defined by $\frac{\mathrm{d}Y_{i\to k}}{\mathrm{d}t} = N_i\frac{Y_i^{N_i}Y_j^{N_j}}{N_i!N_j!}[ij]_k$, which decreases the abundance of nucleus i. $\frac{\mathrm{d}Y_{k\to i}}{\mathrm{d}t} = N_i\frac{Y_l^{N_l}Y_k^{N_k}}{N_l!N_k!}[lk]_i$ is the reaction backward flow, which increases the abundance of nucleus i. The reaction forward and backward flux are the time-integrated reaction forward and backward flow, respectively.

The reaction network and the calculated reaction net fluxes are shown in Fig. 7, where the reaction fluxes are presented by the thickness and type of lines. The reaction fluxes responsible for ^{6}Li, ^{7}Li and ^{7}Be are also listed in Table 2. One can see that the ^{7}Be(d, ^{3}He)^{6}Li reaction net flux is the smallest.

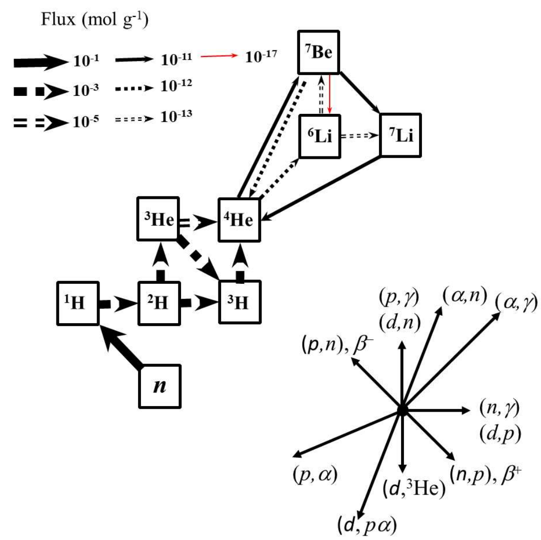

Fig. 7. (color online) The reaction network and the calculated reaction net fluxes.

Table 2. The calculated forward, backward and net fluxes involving ^{6}Li, ^{7}Li and ^{7}Be in the present network. The unit of the fluxes is g^{-1}mol.

reaction	net flux	forward flux	backward flux	Ref.
^{2}H(α, γ)^{6}Li	1.39×10^{-10}	1.39×10^{-10}	3.13×10^{-13}	[38]
^{3}H(α, γ)^{7}Li	8.17×10^{-09}	8.18×10^{-09}	9.13×10^{-12}	[39]
^{3}He(α, γ)^{7}Be	7.17×10^{-11}	7.94×10^{-11}	7.70×10^{-12}	[39]
^{6}Li(n, γ)^{7}Li	1.97×10^{-14}	1.97×10^{-14}	4.85×10^{-31}	[40]
^{6}Li(n, α)^{3}H	7.94×10^{-11}	7.94×10^{-11}	2.49×10^{-26}	[41]
^{6}Li(p, γ)^{7}Be	1.11×10^{-15}	1.35×10^{-15}	2.41×10^{-16}	[42]
^{6}Li(p, α)^{3}He	5.83×10^{-11}	5.83×10^{-11}	7.49×10^{-27}	[43]
^{6}Li(d,n)^{7}Be	7.26×10^{-13}	7.26×10^{-13}	2.52×10^{-18}	[44]
^{6}Li(d, p)^{7}Li	7.26×10^{-13}	7.26×10^{-13}	2.24×10^{-18}	[44]
^{7}Li(p, α)^{4}He	7.49×10^{-09}	7.49×10^{-09}	0.00	[39]
^{7}Li(d,n)2^{4}He	7.50×10^{-10}	7.50×10^{-10}	0.00	[41]
^{7}Be → ^{7}Li	1.13×10^{-13}	1.13×10^{-13}	0.00	[36]
^{7}Be(n, p)^{7}Li	6.39×10^{-11}	6.39×10^{-11}	7.74×10^{-15}	[39]
^{7}Be(n, α)^{4}He	1.85×10^{-12}	1.85×10^{-12}	1.40×10^{-45}	[41]
^{7}Be(d, p)2^{4}He	3.38×10^{-13}	3.38×10^{-13}	0.00	[41]
^{7}Be(d, ^{3}He)^{6}Li	1.11×10^{-17}	1.11×10^{-17}	1.52×10^{-20}	present

Comparing ^{7}Be(d, ^{3}He)^{6}Li with ^{7}Be(d, p)2^{4}He, both of their reverse reactions can be neglected, and the ratio of their reaction flows is equal to the ratio of their reaction rates. Their reaction rates are shown in Fig. 8 together with their flows. The reaction rate of ^{7}Be(d, ^{3}He)^{6}Li is much smaller than that of ^{7}Be(d, p)2^{4}He, and therefore the role of the former in reducing the primordial ^{7}Li abundance is less than that of the latter. As discussed in the introduction, if the ^{7}Be(d, ^{3}He)^{6}Li reaction rate is the same as the ^{7}Be(d, p)2^{4}He reaction rate, it can affect the abundances of ^{7}Li and ^{6}Li by about 1%. Our experiment shows that the reaction rate of ^{7}Be(d, ^{3}He)^{6}Li is much smaller than that of ^{7}Be(d, p)2^{4}He. Therefore, the ^{7}Be(d, ^{3}He)^{6}Li reaction affects the abundances of ^{7}Li and ^{6}Li much less than 1%.

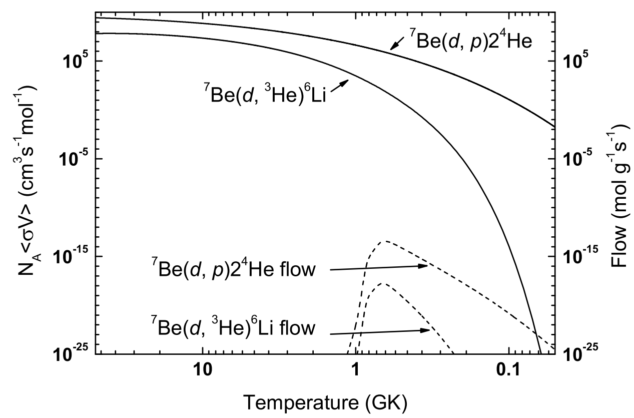

Fig. 8. The ^{7}Be(d, ^{3}He)^{6}Li and ^{7}Be(d, p)2^{4}He [41] reaction rates and flows for temperatures of 0.05 - 50 GK.

The flows creating and destroying ^{6}Li are compared and shown in Fig. 9, where the black solid line and blue dashed line indicate the reactions creating ^{6}Li, while the others are the reactions destroying it. There are only two reactions, ^{2}H(α, γ)^{6}Li and ^{7}Be(d, ^{3}He)^{6}Li, creating ^{6}Li. While the flow of the ^{7}Be(d, ^{3}He)^{6}Li reaction is much smaller than that of ^{2}H(α, γ)^{6}Li, the difference in the fluxes is about 7 orders of magnitude. There are six reactions responsible for destroying ^{6}Li, among which ^{6}Li(n, α)^{3}H and ^{6}Li(p, α)^{3}He are the two main reactions. At higher temperatures, ^{6}Li(n, α)^{3}H is more important than ^{6}Li(p, α)^{3}He because of its higher reaction rate. At lower temperatures, there are few neutrons left because of its decay, and therefore the flow of the ^{6}Li(p, α)^{3}He reaction is bigger than that of ^{6}Li(n, α)^{3}H. The contributions of the ^{6}Li(d, p)^{7}Li and ^{6}Li(d,n)^{7}Be reactions are the same, because identical reaction rates are adopted. Their total contribution is about 1%. The contributions of the ^{6}Li(n, γ)^{7}Li and ^{6}Li(p, γ)^{7}Be reactions are less than one thousandth, which can be neglected.

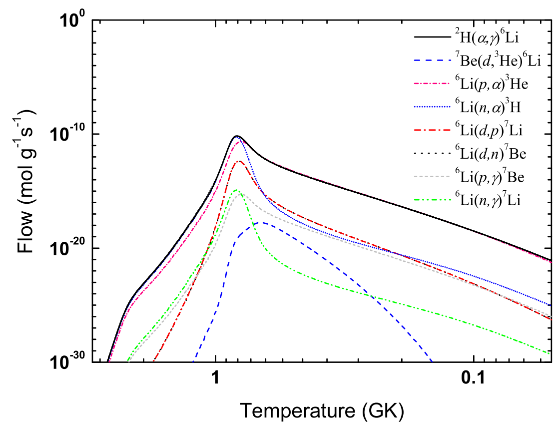

Fig. 9. (color online) Flows of the reactions which create or destroy ^{6}Li. The black solid line and blue dashed line indicate the reactions creating ^{6}Li, while the others are the reactions destroying it.

5 Conclusions

The angular distributions of the ^{2}H(^{7}Be, ^{6}Li)^{3}He reaction were measured with secondary ^{7}Be beams of energy 30.2 MeV and 17.7 MeV for the first time. The integrated cross sections are found to be 73.3 $\pm$ 22.1 mb and 73.1 $\pm$ 15.8 mb at $E_{\rm cm} = 4.0$ MeV and 6.7 MeV, respectively. The excitation function of the ^{7}Be(d, ^{3}He)^{6}Li reaction was determined by normalizing the TALYS calculation with the experimental cross sections, and then its reaction rate was deduced.

To investigate the effect of the ^{7}Be(d, ^{3}He)^{6}Li reaction on the ^{6}Li and ^{7}Li abundances, SBBN network calculations were performed. The results show that the ^{7}Be(d, ^{3}He)^{6}Li reaction has a minimal effect on the abundances of ^{6}Li and ^{7}Li compared with other larger net fluxes such as ^{2}H(α, γ)^{6}Li, ^{7}Be(n, p)^{7}Li and ^{7}Be(d, p)2^{4}He etc. Therefore, the ^{7}Be(d, ^{3}He)^{6}Li reaction is generally ruled out by this experiment as a possible reaction path to alleviate the lithium discrepancy, because of its small reaction rate. The effective temperature of the ^{7}Be(d, ^{3}He)^{6}Li reaction is under 10^9 K and the Gamow window will be below 0.3 MeV. If there is a resonance state between 16.8 and 16.5 MeV in ^{9}B, the reaction rate of the ^{7}Be(d, ^{3}He)^{6}Li reaction could be increased greatly, but at present, no such state has been found [45].

The authors thank the staff of the HI-13 tandem accelerator for their help during the experiment.

References

1 F. Spite and M. Spite, Astron. Astrophys., **115**: 357 (1982)
2 L. M. Hobbs and D. K. Duncan, Astrophys. J, **319**: 796 (1987)
3 A. M. Boesgaard, A. Stephens, and C. P. Deliyannis, Astrophys. J, **633**: 398 (2005)
4 C. Charbonnel and F. Primas, Astron. Astrophys., **442**: 961 (2005)
5 P. Bonifacio, P. Molaro, T. Sivarani et al, Astron. Astrophys., **462**: 851 (2007)
6 J. I. González Hernández, P. Bonifacio, H. -G. Ludwig et al, Astron. Astrophys., **480**: 233 (2008)
7 W. Aoki, P. S. Barklem, T. C. Beers et al, Astrophys. J, **698**: 1803 (2009)
8 A. Hosford, S. G. Ryan, A. E. García Pérez et al, Astron. Astrophys., **493**: 601 (2009)
9 M. Asplund, D. L. Lambert, P. E. Nissen et al, Astrophys. J, **644**: 229 (2006)
10 V. V. Smith, D. L. Lambert, P. E. Nissen, Astrophys. J, **408**: 262 (1993)
11 R. Cayrel, M. Spite, F. Spite et al, Astro. Astrophys., **343**: 923 (1999)
12 P. E. Nissen, D. L. Lambert, F. Primas et al, Astron. Astrophys., **348**: 211 (1999)
13 A. E. García Pérez, W. Aoki, S. Inoue et al, Astron. Astrophys., **504**: 213 (2009)
14 G. Hinshaw, D. Larson, E. Komatsu et al, Astrophys. J, **208**: 19(S) (2013)
15 R. H. Cyburt, B. D. Fields, K. A. Olive et al, Cosm. & Astro. Phys. J, **11**: 12(S) (2008)
16 J. Dunkley, E. Komatsu, M. R. Nolta et al, Astrophys. J, **180**: 306(S) (2009)
17 F. Iocco, G. Mangano, G. Miele et al, Phys. Rep., **472**: 1 (2009)
18 E. Vangioni-Flam, K. A. Olive, B. D. Fields et al, Astrophys. J, **585**: 611 (2003)
19 F. Spite, M. Spite, Proc. IAU Symposium eds. C. Charbonnel, M. Tosi, F. Primas, C. Chiappini, No. 268 (2010)
20 M. A. Famiano, A. B. Balantekin and T. Kajino, Phys. Rev. C, **93**: 045804 (2016)
21 R. H. Cyburt, B. D. Fields, K. A. Olive et al, Rev. Mod. Phys., **88**: 015004 (2016)
22 S. Q. Hou, J, J, He, A. Parikh et al, Astrophys. J, **2**: 834 (2017)
23 A. Coc, E. Vangioni-Flam and P. Descouvemont, Astrophys. J, **600**: 544 (2004)
24 C. Angulo, E. Casarejos, M. Couder et al, Astrophys. J, **630**: 105(L) (2005)
25 R. H. Cyburt and M. Pospelov, Mod. Phys. E, **21**: 1250004 (2012)
26 A.J, Koning, S. Hilaire and M.C. Duijvestijn, "TALYS-1.0", Proc. of the Int. Conf. on Nuclear Data for Science and Technology - ND2007, April 22-27 (2007) Nice, France, eds. O. Bersillon, F. Gunsing, E. Bauge, R. Jacqmin and S. Leray, EDP Sciences, p. 211-214 (2008)
27 W. P. Liu, Z. H. Li, X. X. Bai et al, Nucl. Instrum. Methods B, **204**: 62 (2003)
28 Z. H. Li, B. Guo, S. Q. Yan et al, Phys. Rev. C, **74**: 035801 (2006)
29 E. T. Li, Z. H. Li, Y. J, Li et al, Phys. Rev. C, **90**: 067601 (2014)
30 E. T. Li, B. Guo, Z. H. Li et al, Chin. Phys. C, **40**: 21 (2016)
31 M. Igarashi et al, Computer Program TWOFNR (Surrey University version)
32 I. Brida, S. C. Pieper and R. B. Wiringa, Phys. Rev. C, **84**: 024319 (2011)
33 S. Goriely, S. Hilaire and A. J. Koning, Astron. Astrophys., **487**: 767 (2008)
34 F.-K. Thielemann, M. Arnould and J, Truran, in Advances in Nuclear Astrophysics, edited by A. Vangioni-Flam (Editions Frontiére, Gif-sur-Yvette, France, 1987), p. 525
35 C. M. Perey and F. G. Perey, Atomic Data and Nuclear Data Tables, **17**: 1 (1976)
36 G. Audi, F.G. Kondev, M. Wang et al, Chin. Phys. C, **41**: 030001 (2017)
37 R. V. Wagoner, Astrophys. J, **162**: 247(S) (1969)
38 M. Anders, D. Trezzi, R. Menegazzo et al, Phys. Rev. Lett., **113**: 042501 (2014)
39 P. Descouvemont, A. Adahchour, C. Angulo et al, Atomic Data and Nuclear Data Tables, **88**: 203 (2004)
40 J. Su, Z. H. Li, B. Guo et al, Chin. Phys. Lett., **27**: 052101 (2010)
41 G. R. Caughlan and W. A. Fowler, Atomic Data and Nuclear Data Tables, **40**: 283 (1988)
42 J. J. He, S. Z. Chen, C. E. Rolfs et al, Phys. Lett. B, **725**: 287 (2013)
43 Y. Xu, K. Takahashi and S. Goriely, Nucl. Phys. A, **918**: 61 (2013)
44 D. Thomas, D. N. Schramm, K. A. Olive and B. D. Fields, Astrophys. J, **406**: 569 (1993)
45 P. D. O'Malley, D. W. Bardayan, A. S. Adekola et al, Phys. Rev. C, **84**: 042801(R) (2011)